The effect of coronary bifurcation and haemodynamics in prediction of atherosclerotic plaque development: a serial computed tomographic coronary angiographic study

Antonis Sakellarios[1], PhD; Christos V. Bourantas[2,3], MD, PhD; Stella-Lida Papadopoulou[4,5], MD; Pieter H. Kitslaar[5], MSc; Chrysafios Girasis[4], MD, PhD; Gregg W. Stone[6], MD; Johan H.C. Reiber[5], PhD; Lampros K. Michalis[7], MD, MRCP; Patrick W. Serruys[4], MD, PhD; Pim J. de Feyter[4,5], MD, PhD; Hector M. Garcia-Garcia[8], MD, PhD; Dimitrios I. Fotiadis[1]*, PhD

1. Unit of Medical Technology and Intelligent Information Systems, Department of Materials Science and Engineering, University of Ioannina, Ioannina, Greece; 2. Department of Cardiovascular Sciences, University College London, London, United Kingdom; 3. Department of Cardiology, Barts Heart Centre, London, United Kingdom; 4. Department of Interventional Cardiology, Erasmus University Medical Center, Thoraxcenter, Rotterdam, the Netherlands; 5. Division of Image Processing, Department of Radiology, Leiden University Medical Center, Leiden, the Netherlands; 6. Columbia University Medical Center, New York, NY, USA; 7. Department of Cardiology, Medical School, University of Ioannina, Ioannina, Greece; 8. Interventional Cardiology, MedStar Washington Hospital Center, Washington, DC, USA

GUEST EDITOR: Jolanda J. Wentzel, PhD; *Department of Cardiology, Erasmus MC, Rotterdam, the Netherlands*

Abstract

Aims: The aim of this study was to examine the effect of the daughter branches on the haemodynamics and the potential prediction of atherosclerotic plaque development as well as the best flow division model for accurate blood flow modelling.

Methods and results: We analysed computed tomography coronary angiography retrospective data portraying 17 coronary artery bifurcations in 15 patients recruited into the PROSPECT MSCT study. Baseline and three-year follow-up imaging data were used to reconstruct coronary artery anatomy. In the baseline models blood flow simulations were performed using three flow division approaches: stress-free, Murray's law and Doriot's fit. Blood flow simulation was also performed omitting the daughter branch. The association between ESS estimated in models that incorporated the daughter branches and lumen reduction was higher than the cases where the side branch was omitted. Murray's law provides the most accurate results when comparing the different flow division models. More specifically, low ESS is a predictor of significant lumen reduction (p=0.007), plaque burden increase (p=0.0006) and necrotic core change (p=0.025).

Conclusions: The ESS distribution in coronary models including the daughter branches and based on the calculations implementing Murray's law allows more accurate prediction of atherosclerotic evolution than ESS estimated in models including only the main vessel.

Corresponding author: Unit of Medical Technology and Intelligent Information Systems, Department of Materials Science and Engineering, University of Ioannina, PO BOX 1186, GR 451 10 Ioannina, Greece. E-mail: fotiadis@cc.uoi.gr

Abbreviations

3D   three-dimensional
AHA   American Heart Association
CTCA   computed tomography coronary angiography
ESS   endothelial shear stress
LAD   left anterior descending
LCX   left circumflex artery
RCA   right coronary artery

Introduction

Cardiovascular disease is one of the most common causes of death regulated by systemic factors but also presenting focal manifestations[1]. Atherosclerotic lesions are seen more often in segments with flow disturbances and low endothelial shear stress (ESS), such as in coronary bifurcations and in the inner side of curved vessels, while low ESS is associated with atherosclerotic disease progression and future adverse cardiovascular events[2,3]. Coronary reconstruction in these studies was restricted to the main vessel and did not include the side branches, thus it was not possible to assess the effect of flow division on atherosclerotic evolution. Recently, van der Giessen et al developed a methodology for reconstruction of the main vessel and daughter branches by fusing intravascular and angiographic imaging data[4]. It was demonstrated in 21 patients that the ESS distribution differed in segments in which they incorporated side branches from those in which they did not incorporate the side branches[5]. Reports have shown that computed tomography coronary angiography (CTCA) appears able to assess the extent and severity of coronary atherosclerosis and estimate ESS distribution accurately[6,7]. Nevertheless, the value of complex coronary modelling that includes side branches in estimating the ESS and predicting atherosclerotic evolution more accurately is as yet unclear.

The aim of the present study was to analyse serial CTCA imaging data that portray coronary bifurcations, examine whether ESS can predict disease progression more accurately when daughter branches are incorporated in coronary modelling and blood flow simulation, and investigate which model of flow division in coronary bifurcations allows the most accurate prediction of atherosclerotic evolution.

Methods

The rationale of the study design was to perform 3D reconstruction of the coronary bifurcations of the selected population. The aim was then to perform blood flow modelling according to the proposed flow division models and boundary conditions, and finally to perform statistical analysis between the simulation results, baseline characteristics and disease progression, as this is estimated between the follow-up and baseline examinations. The design of the study is shown in **Figure 1**.

STUDIED POPULATION AND IMAGE ACQUISITION

Retrospective data from the patients recruited into the PROSPECT-MSCT study were analysed. The design and inclusion criteria of the study have been previously described[8]. In brief, this study included patients admitted with an acute coronary syndrome who had complete revascularisation followed by IVUS imaging in the non-culprit vessels and then CTCA at baseline and at three-year follow-up. Imaging at baseline was performed using a 64-slice CTCA scanner (SOMATOM Sensation 64; Siemens Medical Solutions, Forchheim, Germany), while at follow-up a 64-slice dual-source CT scanner (SOMATOM Definition; Siemens Medical Solutions) was used. The acquisition protocol has been presented previously[9]. In total, 36 patients underwent the follow-up protocol, while 58 arteries were finally reconstructed.

1st STEP: 3D RECONSTRUCTION AND REGISTRATION	2nd STEP: BLOOD FLOW MODELLING	3rd STEP: STATISTICAL ANALYSIS
Selection of patient cases from PROSPECT-MSCT database	Estimation of blood flow rate from angiographic images	Division of arteries into 3 mm segments
3D reconstruction of baseline	Measurement of branch diameters	Estimation of plaque area change, lumen area change and plaque burden change
3D reconstruction of follow-up	Estimation of flow rates at the branches using Murray's law and Doriot's fit	Estimation of plaque components change
Plaque components characterisation	Blood flow modelling for four scenarios:	Association of baseline measurements with disease progression
Co-registration of baseline with follow-up	1. Murray's law 2. Doriot's fit 3. Stress-free 4. Segment without side branch	

Figure 1. *Study design. Initially, CTCA data from the PROSPECT-MSCT database were acquired and used for 3D reconstruction. Then blood flow modelling was performed and, finally, statistical analysis was carried out to identify predictors of disease progression.*

From these cases, 17 arteries also included the side branch, which were finally selected for the current study: seven were left anterior descending arteries (LAD), six were right coronary arteries (RCA) and four were left circumflex arteries (LCX). From the LAD arteries, six side branches were classified as 9 and one as 1 according to the American Heart Association (AHA) classification. The side branches of the LCX arteries are classified as 12 according to the AHA. In the RCA arteries, the side branches are located between segments one and two. The average length was 65.8±31.7 mm and 22.8±4.6 mm of the main arteries and the side branches, respectively. All patients provided written informed consent before being recruited into the study.

The acquired CTCA data were processed using the QAngio® CT Research Edition, version 2.0.3 system (Medis Specials, Leiden, the Netherlands) and analysed offline by an experienced operator[8] **(Figure 2)**. The registration between the baseline and follow-up CTCA examinations was performed using anatomical landmarks such as the daughter branches. The plaque characterisation of necrotic, fibrous, fibro-fatty and calcified tissue was achieved using the validated methodology implemented in de Graaf et al[10]. In this methodology, the Hounsfield unit thresholds and the lumen attenuation values are utilised for the definition of the plaque components. The analysis includes only large daughter branches (lumen diameter >1.5 mm, length >20 mm) which originate from the epicardial coronary segments.

RECONSTRUCTION OF CORONARY ANATOMY
The detected lumen and outer wall borders were used for three-dimensional (3D) surface mesh representations. First, the straightened transformed images were converted back into their original orientations in order to calculate an implicit volume function. For each main and daughter branch an implicit volume function was extracted, where their merger was used to construct the coronary segment including the daughter branch. In a final step, the lumen and outer wall surfaces were generated and were treated using smoothing functions **(Figure 3A, Figure 3B)**.

BLOOD FLOW AND BOUNDARY CONDITIONS
The Navier-Stokes equations were employed for blood flow modelling and estimation of the ESS (CFX 14.5; ANSYS, Inc., Canonsburg, PA, USA). The blood was assumed to be a homogeneous, Newtonian fluid with a dynamic viscosity of 0.0035 Pa·s and a density of 1,050 kg/m^3. Blood flow was considered to be laminar and incompressible with a steady flow profile. Zero pressure conditions were applied at the inlet. Two angiographic runs acquired during PCI were used to define patient-specific coronary blood flow. The velocities were then used for the calculation of the flow rate using the area of the inlet boundary. The arterial wall was considered to be rigid and no-slip conditions were applied.

Three different flow division models were used to define a flow rate boundary condition at the outlet of the daughter branches. The first model assumed a stress-free profile with zero pressure boundary condition. The second model implemented Murray's law to estimate flow in the side branches of the bifurcations assuming that the flow ratio through the side branches depends on the ratio of the diameter of the side branches to the third power[11] given by:

$$\frac{q_{D2}}{q_{D1}} = \left(\frac{d_{D2}}{d_{D1}}\right)^3, \tag{1}$$

with q_{D1} and q_{D2} the flow through and d_{D1} and d_{D2} the diameters of the branches.
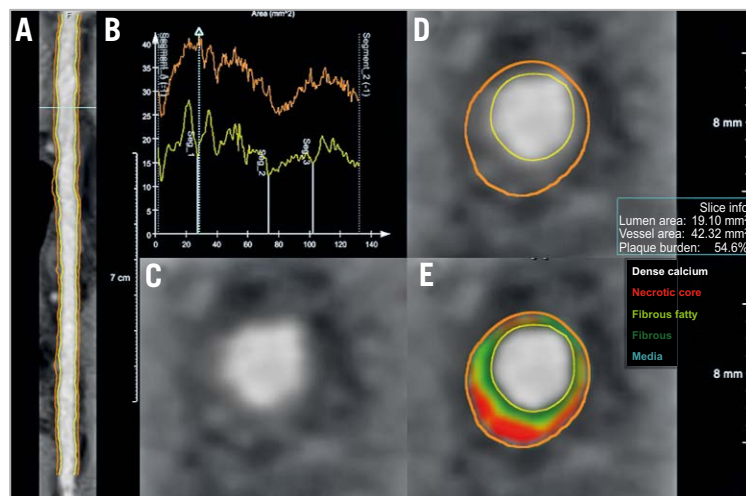
Figure 2. *CTCA data process. A) Initially, the lumen and outer vessel wall borders were detected in the straightened multiplanar reformatted images for baseline and follow-up, respectively. B) Cross-sectional images are generated at 0.5 mm intervals. Gradient magnitude cross-section images (C) are then generated allowing accurate identification of the lumen and outer vessel wall border (D). An automated plaque characterisation method is used for quantification of four tissue types (E). Necrotic core is indicated with a red colour, fibrous fatty with a light green, fibrous with a green colour and calcific tissue with a white colour.*
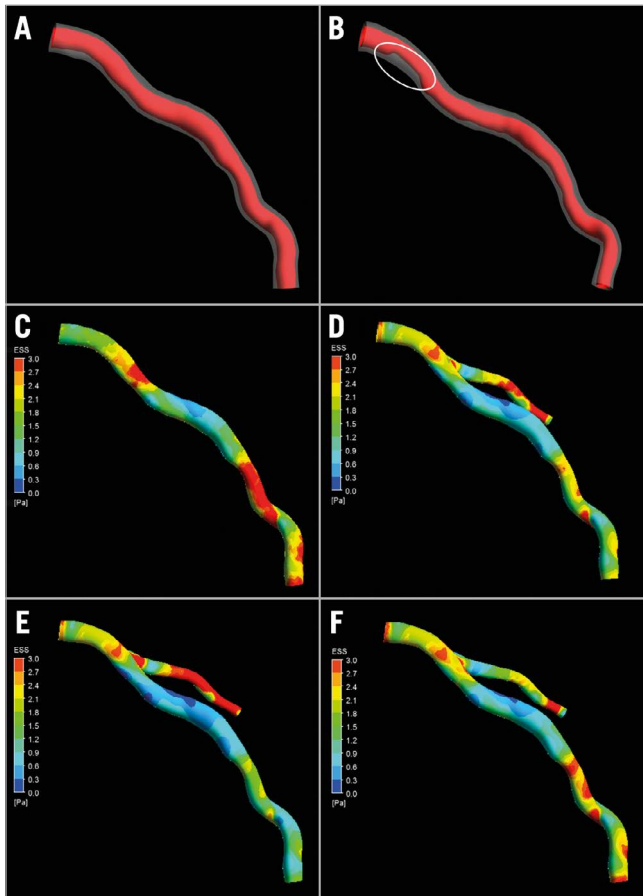
Figure 3. *Example of arterial geometry for baseline (A) and follow-up (B). The white circle depicts the major progress of stenosis. C) - F) Endothelial stress for segment, Murray, Doriot and stress-free simulation case, respectively.*

estimated **(Figure 4)**. Then, knowing the total inflow rate, the flow rates at the branches are calculated using equations 1 and 2. Finally, blood flow simulations were also performed in the main vessel omitting the side branch to examine whether the presence of the side branches affects the ESS and whether an incomplete coronary reconstruction would affect the accuracy of haemodynamics in predicting atherosclerotic evolution.

DATA AND STATISTICAL ANALYSIS

Baseline and follow-up geometries were divided into 3 mm segments. This has traditionally been used to examine the association between ESS plaque characteristics and disease progression[2]. For each segment, the mean lumen area, the mean outer vessel wall area, the mean plaque area, the mean plaque burden (calculated as: 100x mean plaque area/mean outer vessel wall area), the mean composition of the plaque (necrotic core, fibro-fatty, fibrous and calcific tissue area) and the percentage of each plaque component as well as the local minimum averaged ESS in an arc of 90° were estimated[2].

The predominant ESS values were divided into tertiles using the values of the entirety of all arteries to classify the 3 mm subsegments into those exposed to low, moderate and high ESS in each simulation scenario **(Table 1)**. The baseline characteristics of these groups were compared using the Kruskal-Wallis H test for continuous variables and the chi-squared test for categorical variables. Linear and binary logistic regression analyses were performed to investigate associations between ESS and changes of lumen, plaque area and burden, and plaque characteristics at follow-up. We defined a significant change in lumen area as

The third model was based on Doriot's fit[12] and takes into account the combination of the diameter and flow measurements in human coronary arteries:

$$\frac{q_{D2}}{q_{D1}} = \left(\frac{d_{D2}}{d_{D1}}\right)^{2.27}. \tag{2}$$

In order to implement Murray's law and Doriot's fit, the diameters of cross-sections of the branches after the bifurcation are

Table 1. ESS categories for all simulation results.

Simulation type	ESS categories		
	Low	**Moderate**	**Higher**
Murray	<1.11 Pa	(≥1.11 Pa and <1.77 Pa)	≥1.77 Pa
Doriot	<1.09 Pa	(≥1.09 Pa and <1.66 Pa)	≥1.66 Pa
Stress-free	<1.02 Pa	(≥1.02 Pa and <1.56 Pa)	≥1.56 Pa
Artery without daughter branch	<1.15 Pa	(≥1.15 Pa and <1.77 Pa)	≥1.77 Pa
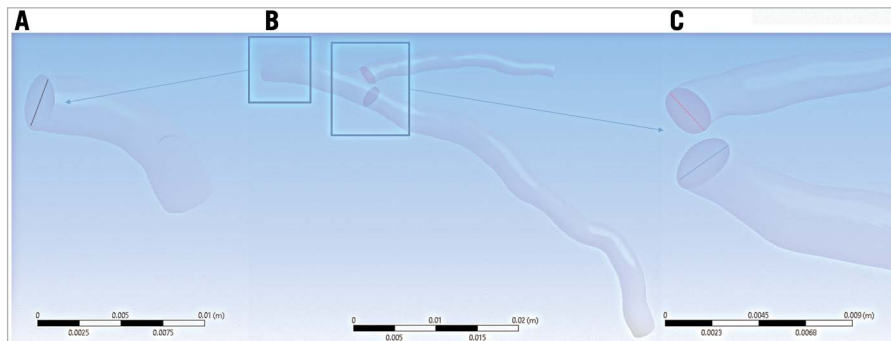
Figure 4. *Use of Murray's law. Initially the inlet diameter and area are calculated (A). Then the areas of cross-sections of the branches after the bifurcation are estimated (B) and, finally, the diameters of the branches are calculated (C).*

a decrease >14.5% from baseline (2 SD of the inter-observed variability of the expert who performed the analysis). Similarly, the 2 SD cut-off was used to define a significant plaque progression as an increase >14.7% of the plaque burden at follow-up. The values of the necrotic core change of the studied 3 mm segments were divided into quarters accordingly, and the upper quarter was used to define a substantial increase in the necrotic core. This was done because the 2 SD of necrotic core change is too low and could not be selected as an accurate cut-off threshold. To control for patient effect, a mixed model with random intercept and slope was used[13]. SAS version 9.3 (SAS Institute, Cary, NC, USA) software was used to perform the statistical analysis. A p-value <0.05 was considered statistically significant.

Results

Fifteen patients who had CTCA that enabled comprehensive assessment of coronary bifurcations (17 coronary arteries) at baseline and at three-year follow-up were included in the current analysis. The baseline characteristics of the studied patients are shown in **Table 2**. All the patients received dual antiplatelet treatment and routine standard of care therapy including statins at discharge. As is shown in **Table 3**, disease progression was noted at follow-up as the plaque area and the necrotic core component were increased at this time point. A typical example of blood flow simulations and ESS results is shown in **Figure 3C**-**Figure 3F**. There were small differences between the different simulation scenarios in the predominant ESS distribution in the 3 mm segments located proximally to the bifurcation segments. On the other hand, the differences of ESS distribution were higher in the main vessel distal to the bifurcation.

Table 4 shows the associations between the changes in lumen area, plaque burden and necrotic core component and the baseline ESS estimated in different simulations. Low ESS at baseline was associated with a reduction in lumen area irrespective

Table 2. Baseline demographics of the studied population.

	Study population (N=15)
Age (years)	52 (44-60)
Sex (male)	14 (93%)
Hypertension	7 (47%)
Dyslipidaemia	3 (20%)
Diabetes mellitus	2 (13%)
History of tobacco use	9 (60%)
Clinical presentation	
Myocardial infarction	12 (80%)
Unstable angina	4 (27%)
Lipid profile	
Total cholesterol (mg/dl)	187 (147-227)
HDL-cholesterol (mg/dl)	45 (32-59)
LDL-cholesterol (mg/dl)	134 (89-178)
Triglycerides (mg/dl)	128 (50-206)

Table 3. Luminal, outer vessel wall and plaque dimensions and characteristics of the 3 mm segments at baseline and at follow-up.

	Baseline	Follow-up	*p*-value
Lumen area (mm²)	10.82 (5.57-16.06)	11.11 (5.64-16.57)	<0.0001
Outer vessel wall area (mm²)	21.17 (14.29-28.05)	21.91 (14.59-29.22)	<0.0001
Plaque area (mm²)	10.36 (7.87-12.84)	10.80 (8.09-13.50)	<0.0001
Plaque burden (%)	50.94 (41.80-60.09)	51.57 (41.83-61.32)	<0.0001
Necrotic core area (mm²)	3.04 (2.19-3.89)	3.48 (2.27-4.70)	<0.0001
Fibro-fatty area (mm²)	2.70 (1.86-3.53)	2.83 (1.98-3.68)	<0.0001
Fibrous area (mm²)	4.22 (2.41-6.02)	3.99 (2.19-5.80)	<0.0001
Calcific area (mm²)	0.25 (-0.38-0.87)	0.34 (-0.47-1.15)	<0.0001

of the flow division model. On the other hand, univariate linear regression analysis demonstrated an association between baseline ESS and plaque burden increase in the model without the daughter branch (p<0.0001), Murray's model (p=0.0034) and Doriot's model (p=0.0175), but not in the stress-free model. Necrotic core increase was correlated with baseline ESS in the Murray's law model (p=0.035) and the stress-free model but not in the model without the side branch. Finally, the increase of fibro-fatty area was associated with baseline ESS in the Murray's law model (p=0.0023), the Doriot's model (p=0.0105), and in the model without the side branch (p=0.0197). None of the calculated ESS models was associated with the increase of the fibrous area.

The results of the univariate binary logistic analysis are shown in **Table 5**. Only the low ESS estimated in the Murray's law model appeared as a predictor of significant lumen reduction (p=0.007), plaque burden increase (p=0.0006) and necrotic core increase (p=0.025). Low ESS in Doriot's model was a predictor of lumen reduction and plaque burden increase but not of necrotic core increase, while low ESS estimated in the stress-free models predicted only the lumen reduction. Finally, low ESS in the model without the daughter branches was only a predictor of substantial lumen decrease and plaque burden increase at follow-up.

Discussion

In the present analysis, we investigated the effect of the side branches on ESS distribution in the main vessel and the effect of different flow division models in predicting disease progression in a retrospective data set of 17 coronary bifurcations from the PROSPECT-MSCT study. We found that blood flow simulation in models that included the side branches allowed more accurate prediction of atherosclerotic evolution and that the Murray's law model simulation is the best for predicting changes in lumen dimensions, plaque burden and composition.

Several experimental and invasive imaging-based studies have examined the role of the local haemodynamic forces on atherosclerotic lesion formation and demonstrated that low ESS increases endothelial permeability and causes endothelial dysfunction, resulting in plaque growth[2,3]. Giannopoulos et al performed an *ex vivo* study in five hearts imaged using CTCA in order to demonstrate

Table 4. Univariate analysis of the variables associated with atherosclerotic disease progression.

Dependent variable	Effect	Regression coefficient (95% CI)	p-value
Decrease in lumen area (per 1 mm^2)	Presence of low ESS at baseline using Murray's law	−0.919 (−1.359 to −0.479)	<0.0001
	Presence of low ESS at baseline using Doriot's fit	−0.755 (−0.279 to −1.230)	0.0019
	Presence of low ESS at baseline using stress-free model	−0.869 (−0.393 to −1.346)	0.0004
	Presence of low ESS at baseline in segment without the daughter branch	−1.228 (−0.779 to −1.676)	<0.0001
	Increasing baseline outer vessel wall area (per 1 mm^2)	−0.143 (−0.197 to −0.089)	<0.0001
	Increasing baseline lumen area (per 1 mm^2)	−0.304 (−0.374 to −0.234)	<0.0001
	Increasing baseline plaque burden (per 10%)	1.217 (0.890 to 1.544)	<0.0001
Increase in plaque burden (per 10%)	Presence of low ESS at baseline using Murray's law	−0.201 (−0.067 to −0.336)	0.0034
	Presence of low ESS at baseline using Doriot's fit	−0.175 (−0.320 to −0.031)	0.0175
	Presence of low ESS at baseline in segment without the daughter branch	−0.167 (−0.307 to −0.027)	0.0195
	Increasing baseline lumen area (per 1 mm^2)	0.040 (0.018 to 0.062)	0.0005
	Increasing baseline plaque area (per 1 mm^2)	−0.127 (−0.157 to −0.097)	<0.0001
	Increasing baseline plaque burden (per 10%)	−0.488 (−0.580 to −0.397)	<0.0001
	Baseline % necrotic tissue (per 10% increase)	0.010 (0.004 to 0.016)	0.0010
	Baseline % calcium (per 10% increase)	0.013 (0.001 to 0.024)	0.0270
Increase in necrotic core area (per 1 mm^2)	Presence of low ESS at baseline using Murray's law	−0.218 (−0.015 to −0.420)	0.0350
	Presence of low ESS at baseline using stress-free model	−0.239 (−0.457 to −0.020)	0.0325
	Baseline % necrotic tissue (per 10% increase)	−0.023 (−0.032 to −0.015)	<0.0001

the effect of daughter branches on the distribution of ESS, which indeed changes in case of not including the daughter branch[14].

Although ESS has numerous implications on vessel biology, the predictive value of low ESS especially for plaque progression has been proven only in some studies, while more commonly low ESS is associated with lumen reduction and plaque burden increase[9]. This could be at least partially attributed to the assumptions that are made during modelling. More specifically, the existence of the daughter branches affects the blood flow simulation considerably and thus the distribution of ESS[5,14]. Moreover, blood flow simulation is affected by approximations in the boundary conditions – which are a key factor for determining the local ESS.

Our study is the first to have performed complete coronary reconstruction from CTCA data including side branches to

Table 5. Univariate binary logistic analysis of the variables associated with atherosclerotic disease progression.

Dependent variable	Explanatory variable	Odds ratio (95% CI)	p-value
Lumen reduction	Presence of low ESS at baseline using Murray's law	1.845 (1.181 to 2.883)	0.007
	Presence of low ESS at baseline using Doriot's fit	1.878 (1.209 to 2.918)	0.005
	Presence of low ESS at baseline using stress-free model	2.362 (1.524 to 3.661)	0.0001
	Presence of low ESS at baseline in segment without the daughter branch	1.669 (1.118 to 2.492)	0.012
	Increasing baseline lumen area (per 1 mm^2)	1.240 (1.128 to 1.363)	<0.0001
	Decreasing plaque burden (per 10%)	2.704 (1.671 to 4.375)	<0.0001
Plaque burden increase	Presence of low ESS at baseline using Murray's law	1.979 (1.342 to 2.916)	0.0006
	Presence of low ESS at baseline using Doriot's fit	1.807 (1.198 to 2.727)	0.005
	Presence of low ESS at baseline using stress-free model	1.403 (0.938 to 2.097)	0.099
	Presence of low ESS at baseline in segment without the daughter branch	1.837 (1.287 to 2.621)	0.0008
	Decreasing baseline plaque area (per 1 mm^2)	1.460 (1.157 to 1.844)	0.006
	Decreasing plaque burden (per 10%)	2.781 (1.370 to 5.646)	0.005
Necrotic core increase	Presence of low ESS at baseline using Murray's law	1.626 (1.063 to 2.489)	0.025
	Presence of low ESS at baseline using stress-free model	1.677 (1.059 to 2.656)	0.028
	Increasing baseline % necrotic tissue (per 10%)	1.592 (1.250 to 2.026)	0.0002
	Increasing baseline lumen area (per 1 mm^2)	1.066 (0.997 to 1.139)	0.062
	Increasing baseline % fibro-fatty tissue (per 10%)	1.773 (0.933 to 3.370)	0.081

examine whether the ESS in these models can predict disease progression and investigate which model of flow division in coronary bifurcations provides the most accurate prediction of atherosclerotic evolution. In agreement with previous invasive imaging-based studies, we found that the ESS distribution estimated in models that included side branches was different from the ESS estimated in the models without the side branches[15], and that the local haemodynamic patterns estimated in the complete reconstructions enabled more accurate prediction of atherosclerotic disease progression.

The definition of the boundary conditions is a key factor for reliable calculation of ESS[16]. In our study, we examined three different flow division scenarios and we found that the ESS estimated in models that included the side branches using Murray's law enabled prediction of a decrease in the lumen area, and an increase in the plaque burden and necrotic core component.

Limitations

CTCA imaging was performed at baseline with an earlier-generation 64-slice scanner, which may have produced inferior image quality compared to the dual-probe scanner used at follow-up. Nevertheless, the tube voltage that may affect the performance of the plaque characterisation algorithm was the same in both scans. CTCA has limited accuracy in detecting plaque morphology and composition, while the blooming effect in calcified lesions may not allow accurate delineation of the lumen and outer vessel wall borders. However, in the present study the calcific tissue component was minimal and thus it is very unlikely to have affected the reported results. Another potential of CTCA is the ability to reconstruct the full coronary arterial tree. However, in this work we have included only diameters >1.5 mm and we focus only on the epicardial arteries. As a future work, the authors intend to implement blood flow modelling in coronary arterial trees in order to demonstrate the effect of ESS on disease progression under realistic geometric conditions.

A significant limitation of the present analysis is the small number of patients, which does not allow us to draw conclusions about the value of the ESS estimated in models including the side branches for predicting future adverse cardiovascular events. However, this is an exploratory study and, although we included only a small number of patients in the present analysis, the number of 3 mm segments (n=335) is sufficient to allow us to test the hypothesis of the current study. Moreover, the association of low ESS with plaque progression in a larger population of coronary arteries has already been proven in a previous work[17]. Another limitation of the current study regards the debatable argument about the CTCA capability to identify outer wall and plaque components. Indeed, CTCA has been validated in several studies concerning its accuracy to identify lumen, outer wall and calcified plaque components[10,18,19]. However, it has a limited accuracy to identify lipid tissue. On the other hand, the methodology for the plaque characterisation used in this study has been previously validated.

Conclusions

We performed blood flow modelling in 17 coronary bifurcations applying several kinds of boundary conditions to estimate flow division in coronary bifurcation. The implementation of flow division according to Murray's law for the calculation of ESS allows more accurate prediction of atherosclerosis evolution (lumen area, increase in plaque burden and change in necrotic core) than using only the main vessels. Confirmation of these findings in future pilot studies is needed before conducting a large-scale study that would examine the additive value of the ESS estimated in models that include side branches in predicting lesions that will progress and cause events.

Impact on daily practice

This work proves that accurate computational modelling of blood flow in coronary arteries requires taking the daughter branch into account. Prediction of lumen reduction and plaque burden increase is associated with low ESS regions when the daughter branch is considered in the reconstruction, but also when omitting it from the reconstruction. However, the correlation of low ESS with necrotic core increase is present only when the daughter branch is considered in the simulation.

Guest Editor

This paper was guest edited by Jolanda J. Wentzel, PhD; Department of Cardiology, Erasmus MC, Rotterdam, the Netherlands.

Conflict of interest statement

G. Stone is a consultant for Abbott Vascular, Volcano, and Infraredx. The other authors have no conflicts of interest to declare. The Guest Editor has no conflicts of interest to declare.

References

1. W.H.O. The atlas of heart disease and stroke. http://www.who.int/cardiovascular_diseases/en/cvd_atlas_16_death_from_stroke.pdf

2. Stone PH, Saito S, Takahashi S, Makita Y, Nakamura S, Kawasaki T, Takahashi A, Katsuki T, Nakamura S, Namiki A, Hirohata A, Matsumura T, Yamazaki S, Yokoi H, Tanaka S, Otsuji S, Yoshimachi F, Honye J, Harwood D, Reitman M, Coskun AU, Papafaklis MI, Feldman CL; PREDICTION Investigators. Prediction of progression of coronary artery disease and clinical outcomes using vascular profiling of endothelial shear stress and arterial plaque characteristics: the PREDICTION Study. *Circulation.* 2012;126:172-81.

3. Samady H, Eshtehardi P, McDaniel MC, Suo J, Dhawan SS, Maynard C, Timmins LH, Quyyumi AA, Giddens DP. Coronary artery wall shear stress is associated with progression and transformation of atherosclerotic plaque and arterial remodeling in patients with coronary artery disease. *Circulation.* 2011;124:779-88.

4. van der Giessen AG, Schaap M, Gijsen FJ, Groen HC, van Walsum T, Mollet NR, Dijkstra J, van de Vosse FN, Niessen WJ, de

Feyter PJ, van der Steen AF, Wentzel JJ. 3D fusion of intravascular ultrasound and coronary computed tomography for in-vivo wall shear stress analysis: a feasibility study. *Int J Cardiovasc Imaging.* 2010;26:781-96.

5. Li Y, Gutiérrez-Chico JL, Holm NR, Yang W, Hebsgaard L, Christiansen EH, Maeng M, Lassen JF, Yan F, Reiber JH, Tu S. Impact of Side Branch Modeling on Computation of Endothelial Shear Stress in Coronary Artery Disease: Coronary Tree Reconstruction by Fusion of 3D Angiography and OCT. *J Am Coll Cardiol.* 2015;66:125-35.

6. van der Giessen AG, Wentzel JJ, Meijboom WB, Mollet NR, van der Steen AF, van de Vosse FN, de Feyter PJ, Gijsen FJ. Plaque and shear stress distribution in human coronary bifurcations: a multi-slice computed tomography study. *EuroIntervention.* 2009;4:654-61.

7. van der Giessen AG, Groen HC, Doriot PA, de Feyter PJ, van der Steen AF, van de Vosse FN, Wentzel JJ, Gijsen FJ. The influence of boundary conditions on wall shear stress distribution in patients specific coronary trees. *J Biomech.* 2011;44:1089-95.

8. Papadopoulou SL, Neefjes LA, Garcia-Garcia HM, Flu WJ, Rossi A, Dharampal AS, Kitslaar PH, Mollet NR, Veldhof S, Nieman K, Stone GW, Serruys PW, Krestin GP, de Feyter PJ. Natural history of coronary atherosclerosis by multislice computed tomography. *JACC Cardiovasc Imaging.* 2012;5:S28-37.

9. Sakellarios A, Bourantas CV, Papadopoulou SL, Tsirka Z, de Vries T, Kitslaar PH, Girasis C, Naka KK, Fotiadis DI, Veldhof S, Stone GW, Reiber JH, Michalis LK, Serruys PW, de Feyter PJ, Garcia-Garcia HM. Prediction of atherosclerotic disease progression using LDL transport modelling: a serial computed tomographic coronary angiographic study. *Eur Heart J Cardiovasc Imaging.* 2017;18:11-18.

10. de Graaf MA, Broersen A, Kitslaar PH, Roos CJ, Dijkstra J, Lelieveldt BP, Jukema JW, Schalij MJ, Delgado V, Bax JJ, Reiber JH, Scholte AJ. Automatic quantification and characterization of coronary atherosclerosis with computed tomography coronary angiography: cross-correlation with intravascular ultrasound virtual histology. *Int J Cardiovasc Imaging.* 2013;29:1177-90.

11. Murray CD. The Physiological Principle of Minimum Work Applied to the Angle of Branching of Arteries. *J Gen Physiol.* 1926;9:835-41.

12. Doriot PA, Dorsaz PA, Dorsaz L, De Benedetti E, Chatelain P, Delafontaine P. In-vivo measurements of wall shear stress in human coronary arteries. *Coron Artery Dis.* 2000;11:495-502.

13. Peters J, Reif U. Subdivision Surfaces. Series: Geometry and Computing, Vol. 3. New York, USA: Springer; 2008, XVI.

14. Giannopoulos AA, Chatzizisis YS, Maurovich-Horvat P, Antoniadis AP, Hoffmann U, Steigner ML, Rybicki FJ, Mitsouras D. Quantifying the effect of side branches in endothelial shear stress estimates. *Atherosclerosis.* 2016;251:213-8.

15. Li Y, Gutierrez-Chico JL, Holm NR, Yang W, Hebsgaard L, Christiansen EH, Maeng M, Lassen JF, Yan F, Reiber JH, Tu S. Impact of Side Branch Modeling on Computation of Endothelial Shear Stress in Coronary Artery Disease Coronary Tree Reconstruction by Fusion of 3D Angiography and OCT. *J Am Coll Cardiol.* 2015;66:125-35.

16. Liu BY, Zheng J, Bach R, Tang DL. Influence of model boundary conditions on blood flow patterns in a patient specific stenotic right coronary artery. *Biomed Eng OnLine.* 2015;14(Suppl 1):S6.

17. Bourantas CV, Papadopoulou SL, Serruys PW, Sakellarios A, Kitslaar PH, Bizopoulos P, Girasis C, Zhang YJ, de Vries T, Boersma E, Papafaklis MI, Naka KK, Fotiadis DI, Stone GW, Reiber JH, Michalis LK, de Feyter PJ, Garcia-Garcia HM. Noninvasive Prediction of Atherosclerotic Progression: The PROSPECT-MSCT Study. *JACC Cardiovasc Imaging.* 2016;9:1009-11.

18. Broersen A, de Graaf MA, Eggermont J, Wolterbeek R, Kitslaar PH, Dijkstra J, Bax JJ, Reiber JH, Scholte AJ. Enhanced characterization of calcified areas in intravascular ultrasound virtual histology images by quantification of the acoustic shadow: validation against computed tomography coronary angiography. *Int J Cardiovasc Imaging.* 2016;32:543-52.

19. Obaid DR, Calvert PA, Gopalan D, Parker RA, Hoole SP, West NE, Goddard M, Rudd JH, Bennett MR. Atherosclerotic plaque composition and classification identified by coronary computed tomography: assessment of computed tomography-generated plaque maps compared with virtual histology intravascular ultrasound and histology. *Circ Cardiovasc Imaging.* 2013;6:655-64.